Earth and Space Science

RESEARCH ARTICLE
10.1029/2019EA000961

Gap Filling of Advanced Technology Microwave Sounder Data as Applied to Hurricane Warm Core Animations

Banghua Yan[1], Ding Liang[2], Warren Porter[3], Jingfeng Huang[3], Ninghai Sun[2], Lihang Zhou[4], Tong Zhu[5], Mitch Goldberg[4], Da-Lin Zhang[6], and Quanhua Liu[1]

[1]NOAA/STAR/Satellite Meteorology and Climatology Division, College Park, MD, USA, [2]Global Science Technologies, Inc, Greenbelt, MD, USA, [3]Science Systems and Applications, Inc, Greenbelt, MD, USA, [4]NOAA/JPSS Program Science Office, Greenbelt, MD, USA, [5]IM Systems Group, Inc, Rockville, MD, USA, [6]Department of Atmospheric and Oceanic Science, University of Maryland, College Park, MD, USA

Key Points:
- This study fills orbital gaps within ATMS Sensor Data Record (SDR) data to visually observe whole hurricane warm core structures
- This study establishes a 3-D Hurricane Warm Core Animation System (HWCAS) from near real-time ATMS observations
- Each 3-D animation contains 97 2-D atmospheric temperature anomaly images at different cross-sections through hurricane core regions

Correspondence to:
B. Yan,
banghuayan@noaa.gov

Citation:
Yan, B., Liang, D., Porter, W., Huang, J., Sun, N., Zhou, L., et al. (2020). Gap filling of advanced technology microwave sounder data as applied to hurricane warm core animations. *Earth and Space Science*, *7*, e2019EA000961. https://doi.org/10.1029/2019EA000961

Received 21 OCT 2019
Accepted 30 JUL 2020
Accepted article online 3 AUG 2020

Abstract As a microwave radiometer seeing through clouds, Advanced Technology Microwave Sounder (ATMS) observations play a critical role in visually monitoring hurricane warm core structures. However, the presence of orbit gaps within the ATMS observations at low latitudes regions, where hurricanes frequently develop, raises concerns in monitoring hurricanes' spatial variability. To resolve this issue, this study generates gap-filled ATMS brightness temperature data by using the smoothing algorithm of Penalized Least Square Discrete Cosine Transform. The accuracies of the missing-filled brightness temperatures for temperature sounding channels are approximately within 1 K. Furthermore, the gap-filled brightness temperature data from channels 5–12 are utilized to establish a three-dimensional Hurricane Warm Core Animation System (HWCAS) in near real time (NRT), which helps to visually observe realistic warm core structures of a hurricane system. The information of hurricane warm core over open oceans and coastal areas is derived using a combination of three new regression-based atmospheric temperature retrieval algorithms, with the averaged error typically within ±1 K at the vertical levels a warm core could occur. Each animation consists of 97 two-dimensional atmospheric temperature anomaly images at different cross-sections through hurricane core regions. The retrieved maximum temperature anomalies show well the formation, intensification, weakening, reintensification, and dissipation stages of Hurricane Florence that are similar to those from the European Centre for Medium-Range Weather Forecasts (ECMWF) analysis. They also show similar weakening and reintensifying stages to those of the maximum sustained winds by the best track data, albeit with some temporal lead/lag. With its strength in NRT hurricane monitoring, the HWCAS demonstrate its great potential in providing meteorologists with timely information of temperature anomaly fields in the inner-core regions of a hurricane.

1. Introduction

The Advanced Technology Microwave Sounder (ATMS) is a cross-track scanning microwave instrument measuring antenna (brightness) temperatures at 22 channels ranging from 23 to 183 GHz to observe atmospheric temperature and moisture profiles under all weather conditions. The instrument has been flown aboard Suomi National Polar-orbiting Partnership (SNPP) and NOAA-20, formerly Joint Polar Satellite System (JPSS)-1, and will be onboard JPSS-2 through JPSS-4. As shown in Table 1 (Weng et al., 2013), ATMS combines the capabilities of current Advanced Microwave Sounding Unit-A (AMSU-A) and Microwave Humidity Sounder (MHS). The instrument scans as large as ±52.725° at each side of nadir with a total of 96 viewing angles, and it has a scan swath of about 2,700 km which is wider than that of AMSU-A (~2,200 km). Currently, ATMS Sensor Data Record (SDR) data have contributed significantly to Numerical Weather Prediction (NWP) Systems for generating short to medium range (1–10 days) weather forecasts (Kelly & Thépaut, 2017; Tong et al., 2017; Zhu et al., 2017; Zou et al., 2013). The data are also widely used by various satellite-based algorithms to retrieve environmental Earth atmospheric and surface (Boukabara et al., 2011, 2013; Ferraro et al., 2018; Meng et al., 2017; Tian & Zou, 2016; You et al., 2016; Zhu et al., 2002; Zhu & Weng, 2013).

Table 1
Suomi NPP Advanced Technology Microwave Sounder (ATMS) Sensor Characteristics (Weng et al., 2013)

Channel	Center frequency (GHz)	Polarization	FOV (°)	Peak of weighting function
1	23.8	V	5.2	Window (surface)
2	31.4	V	5.2	Window (surface)
3	50.3	H	2.2	Window (surface)
4	51.76	H	2.2	Window (950 hPa)
5	52.8	H	2.2	Low sounding (850 hPa)
6	53.596 ± 0.115	H	2.2	700 hPa
7	54.40	H	2.2	400 hPa
8	54.94	H	2.2	250 hPa
9	55.50	H	2.2	200 hPa
10	57.2903	H	2.2	100 hPa
11	57.2903 ± 0.115	H	2.2	50 hPa
12	57.2903	H	2.2	25 hPa
13	57.2903 ± 0.322	H	2.2	10 hPa
14	57.2903 ± 0.322 ± 0.010	H	2.2	5 hPa
15	57.2903 ± 0.322 ± 0.004	H	2.2	2 hPa
16	87–91 (88.20)	V	2.2	Window (surface)
17	165.5	H	1.1	Near surface
18	183.31 ± 7	H	1.1	800 hPa
19	183.31 ± 4.5	H	1.1	700 hPa
20	183.31 ± 3	H	1.1	500 hPa
21	183.31 ± 1.8	H	1.1	400 hPa
22	183.31 ± 1.0	H	1.1	300 hPa

Note. Peak values of ATMS weighting functions of U.S. standard atmospheric condition are referred to (Weng, 2018).

In particular, atmospheric temperature information about the hurricane warm core is important for meteorologists to monitor and forecast tropical cyclones (TCs) intensity (Dolling & Barnes, 2012; Wang et al., 2010; Zhang & Chen, 2012). ATMS brightness temperature data have been utilized to retrieve vertical warm core structures for a number of TC in a series of legacy of satellite regression retrieval algorithms (Tian & Zou, 2016; Zhu et al., 2002; Zhu & Weng, 2013). In addition to the regression retrieval algorithms, global atmospheric temperature information is retrieved more accurately in some comprehensively satellite retrieval systems such as the National Oceanic and Atmospheric Administration's Microwave Integrated Retrieved System (MiRS) (Boukabara et al., 2011). However, intrinsic gaps between successive orbits of ATMS observations still exist at low latitudes regions (https://www.star.nesdis.noaa.gov/icvs/status_N20_ATMS.php) where TCs frequently occur each year. Although the orbit gap is much narrower than that of its predecessor (i.e., AMSU), the maximum width of the gap is about 250 km for ATMS temperature sounding channels. The size (diameter) of warm core is in the range of 100–300 km, so the small orbit gap in ATMS observations could still be a concern for understanding spatial variability of a TC, especially when the data gap occurs near or within the TC warm core area. In addition to the data accuracy, the time it takes to track the evolution of a TC in intensity and location is also of concern. Hence, a near-real time ATMS-based three-dimension (3-D) animation system that provides hurricane temperature anomaly distributions without gaps is highly desirable and valuable to meteorologists in visually monitoring hurricane intensity, studying its inner core dynamics, and constructing the initial vortex for hurricane simulations.

To meet these needs, in this study, we introduce a new methodology to produce gap-filled ATMS SDR brightness temperature data by using a well-validated smoothing algorithm of Penalized Least Square (PLS) Discrete Cosine Transform (DCT) (Garcia, 2010a, 2010b). The smoothing algorithm requires evenly spaced data; thus, reprocessing of the original ATMS SDR data is needed to grid the data and to correct the angle dependency of brightness temperature due to the limb effect (Zhang et al., 2017). The accuracy of gap-filled brightness temperatures is assessed by applying the smoothing algorithm to a series of ATMS observations with or without a hurricane event. Secondly, we develop three new regression-based retrieval algorithms to produce vertical atmospheric temperature fields under all weather conditions for a hurricane event over open oceans and coastal areas, by using the gap-filled ATMS SDR data from Channel 5 through Channel 12. The development of the algorithms over open oceans take certain advantages of the original

regression algorithm using the same temperature sounding channels as predictors (Zhu & Weng, 2013, hereafter referred to as ZW13). The algorithm over coastal regions utilizes five ATMS channels from 8 to 12 and is applicable for all weather conditions. Finally, we develop a 3-D image animation system that shows atmospheric temperature anomaly distribution of hurricane warm core structures with the retrieved atmospheric fields.

The next section introduces the methodology of the DCT-PLS smoothing algorithm along with the accuracy assessment of gap-filled brightness temperatures. Section 3 presents the development of three temperature retrieval algorithms and the associated accuracy assessments. Section 4 describes the ATMS-based 3-D Hurricane Warm Core Animation System (HWCAS) in near-real time mode through a case study of Hurricane Florence (2018). A summary and conclusions are given in section 5.

2. Gap-Filling of ATMS SDR Data

2.1. Preprocessing of ATMS SDR Data

Evenly spaced data are prerequisite of using the DCT smoothing algorithm (Garcia, 2010b) to conduct data gap filling. In reality, ATMS satellite observations are measured at a given instantaneous Field-of-View (FOV) that varies with channels. The 5.3°, 2.2°, and 1.1° represent the FOVs of two window channels from 1 to 2, 14 temperature sounding channels from 3 through 16, and six water vapor sounding channels from 17 to 22, respectively. Specifically, the FOV of 2.2° at the temperature sounding channels approximately corresponds to 32 km or 1/3 degree spatial resolution on Earth at nadir and the spatial resolution gradually decreases from nadir to swath edge. Some missing points potentially exist near the swath edges in the gridded ATMS data, because of the large horizontal sampling interval between FOVs at the edges. Some forms of resolution enhancement, such as Backus-Gilbert or Fast Fourier Transformation resampling method, can be used to improve the spatial resolution of two lowest frequency ATMS channels that are oversampled (Yang & Zou, 2014), albeit with the cost of increasing sampling noise. For the warm core analysis in this study, we only use temperature sounding channels, at which channels the impact of surface emissivity and other inhomogeneity for these channels are very limited, and the application of the above enhancement is less needed. In this study, the ATMS SDR data are gridded into 1/3 degree resolution on Earth in favor to the spatial resolution of temperature sounding channels to produce an evenly spaced data in the data preparation. Any "missed" points near the swath edge in the gridded data are merely treated as "gaps" and are filled using the DCT-PLS smoothing algorithm.

On the other hand, the original ATMS observations have a sensor zenith angle range of $\pm 52.725°$ on both sides of the nadir, which poses limb effects towards the scanning swath edges. The limb effect represents changes in the optical path-length through the Earth's atmosphere between the Earth and the satellite. In comparison to the nadir observations, the scan angle-dependent ATMS brightness temperature measurements off nadir could have bias up to 15 K at the extreme scan positions due to the limb effect in the temperature sounding channels, and such limb effect induced bias could be up to 30 K in the window channels (Zhang et al., 2017). Currently, NOAA produces operational limb-corrected ATMS brightness temperature data routinely (https://www.star.nesdis.noaa.gov/jpss/EDRs/products_ATMS_LC.php) (Zhang et al., 2017). To reduce the data uncertainty at large zenith angles, the limb-corrected ATMS SDR data are used instead of the original SDR data to produce the evenly spaced gridded data in the data preparation process before gap filling.

2.2. Gap-Filling Methodology

The gap filling of the gridded limb-corrected ATMS SDR data is performed using the DCT-PLS smoothing algorithm that is widely used for automatic smoothing of multidimensional incomplete data (Garcia, 2010a, 2010b). In comparison to other smoothing algorithms, this algorithm features high flexibility, good maturity, and better accuracy, especially for gap filling of satellite data. An iteratively weighted robust version of the smoothing algorithm in MATLAB for multiple dimensional data sets is available for public use (Garcia, 2010a). More importantly, the algorithm has been successfully extended to the 3-D smoothing to fill in gaps of global satellite soil moisture observations, which clearly demonstrated its capability in filling data gaps in global satellite data set with high accuracy (Wang et al., 2012). The following provides a brief introduction of the smoothing algorithm. Full details of its mathematical explanations can be found in Garcia (2010a, 2010b).

Let X stand for an evenly spaced two-dimensional (2-D) data set for given latitudes and longitudes with missing data, that is, data gaps plus missed pixels at very large scan angles in the gridded data. W is a binary array of the same size indicating whether the values are missing, where $W_{i,j} = 0$ for missing points otherwise $W_{i,j} = 1$. The DCT-PLS seeks for $\widehat{X}$ that minimizes

$$F\left(\widehat{X}\right) = \left\| W^{\frac{1}{2}} \circ \left(\widehat{X} - X\right) \right\|^2 + S\left\| \nabla^2 \widehat{X} \right\|^2, \tag{1}$$

where $\|\|$ denotes the Euclidean norm; ∇^2 and °stand for the Laplace operator and the Schur (elementwise) product. $\widehat{X}$ is achieved by rewriting Equation 1 with the DCT and its inverse DCT (Garcia, 2010a, 2010b)

$$\widehat{X} = IDCT\left(\Gamma \circ DCT\left(W \circ \left(\widehat{X} - X\right) + \widehat{X}\right)\right). \tag{2}$$

Here, the Γ is the diagonal matrix defined by

$$\Gamma_{i_1, i_2} = \left[1 + S\left(\sum_{j=1}^{2}\left(2 - \frac{2\cos\left(i_j - 1\right)\pi}{n_j}\right)\right)^2\right]^{-1} \text{ and } \Gamma_{i,j} = 0 \text{ if } i \neq j, \tag{3}$$

where i_j denotes the ith element along the jth dimension, n_j is the size of X along the jth dimension.

The operators DCT and Inverse Discrete Cosine Transform (IDCT) in Equation 2 stand for the type-II DCT and IDCT, respectively. By following Ahmed et al. (1974); Khayam (2003); and Strang (1999), the expressions of DCT and IDCT elements are briefed below.

For given 2-D data, $y_{i,j}$, which is the element of the vector $\left[W \circ \left(\widehat{X} - X\right) + \widehat{X}\right]$, DCT element, $Y_{u,v}$, is defined by

$$\left(Y_{u,v}\right)_{DCT} = \alpha(u)\alpha(v)\sum_{i=0}^{M-1}\sum_{j=0}^{N-1} y_{i,j}\cos\left[\frac{(2i+1)u\pi}{2M}\right]\cos\left[\frac{(2j+1)v\pi}{2N}\right], \tag{4}$$

and

$$\alpha(u) = \begin{cases} \sqrt{\frac{1}{M}} & for\ u = 0 \\ \sqrt{\frac{2}{M}} & for\ u \neq 0 \end{cases} \text{ and } \alpha(v) = \begin{cases} \sqrt{\frac{1}{N}} & for\ v = 0 \\ \sqrt{\frac{2}{N}} & for\ v \neq 0 \end{cases}, \tag{5}$$

where u,v are discrete variables, with $u = 0, 1, 2, \ldots, M-1$, and $v = 0, 1, 2, \ldots, N-1$.

Correspondingly, the IDCT element, $y_{i,j}$, is given as follows.

$$\left(y_{i,j}\right)_{IDCT} = \sum_{i=0}^{M-1}\sum_{j=0}^{N-1}\alpha(u)\alpha(v)Y_{u,v}\cos\left[\frac{(2i+1)u\pi}{2M}\right]\cos\left[\frac{(2j+1)v\pi}{2N}\right]. \tag{6}$$

In view of Equations 2 and 3, the DCT-PLS method relies on the choice of the smoothing parameter S that is a real positive scalar and controls the degree of smoothing. As the parameter S increases, the smoothness of $\widehat{X}$ also increases. This parameter is estimated using the method of Generalized Cross-Validation (GCV) by minimizing the GCV score, which yields the best estimate of the original data and thus avoids oversmoothing or undersmoothing as much as possible (Craven & Wahba, 1978; Golub et al., 1979; Wahba, 1990). For the ATMS channels in this study, the magnitudes of this parameter vary primarily in the range of 0.1 to 10.0, depending the channel.

Notice that Equation 2 does not give an explicit formula to solve $\widehat{X}$. According to Garcia (2010a), this implicit formula can be solved using an iterative procedure starting with an arbitrary $\widehat{X}(0)$, that is,

$$\widehat{X}(k+1) = IDCT\left(\Gamma \circ DCT\left(W \circ \left(\widehat{X}(k) - X\right) + \widehat{X}(k)\right)\right). \tag{7}$$

The above procedure in MATLAB is available for public (http://www.biomecardio.com/matlab/smoothn_doc.html#2) (Garcia, 2010a).

2.3. Assessment of Gap-Filling ATMS Brightness Temperatures

Figure 1 displays the ATMS brightness temperature images at Channel 7 with/without the use of the smoothing algorithm for observations of four strong TCs in 2018, that is, Hurricane Aletta on 8 June, Hurricane Bud on 12 June, Typhoon Maria on 6 July, and Hurricane Hector on 16 August 2018. Figures 1a–1d show the orbit gaps and some missing values at sensor zenith angles far off the nadir in ATMS observations of these events. Although the gap is narrow, the presence of such small data gaps could still cause concerns for spatial and temporal variability analysis of the hurricanes. Unlike the images in (a) to (d), the gap-filled ATMS images in (e) to (h) demonstrate that the missing values in the images are well filled not only over orbital gaps but also over swath edges with high scanning angles. Therefore, the gap-filled ATMS data can provide full coverage of brightness temperature distributions even in the presence of a hurricane in the data field. It is also noted that the gap filling could cause some residual error due to losing subtle variations of brightness temperature in the original data. Hence, it is important to quantify uncertainties of the gap-filled brightness temperatures.

To evaluate the accuracy of the gap-filled brightness temperatures, we process the ATMS observations of nine hurricanes and 24 nonhurricane cases by artificially setting six pixels of ATMS brightness temperatures per scan each case to missing values to create synthetic artificial gaps. Six missed pixels per scan are selected to mimic the width of ATMS orbit gap. An artificial data set is adopted because it is difficult, if not impossible, to directly measure the uncertainty of filled brightness temperatures among originally missing ATMS observations. The synthetic data gaps are reconstructed using the above-mentioned DCT-PLS method. The original ATMS-measured brightness temperatures are used as "truth" to assess the errors of DCT-predicated brightness temperatures within the artificial gaps as discussed below. Figure 2 displays a box-and-whisker plot of errors at each channel, based on statistical analysis of 33 cases for the synthetic gaps, where an error is equal to the difference between the predicted (the gap-filled) and the measured brightness temperatures. The largest errors occur at surface window channels and surface-sensitive sounding channels. For example, 75% of the errors at the channels from 1 to 4 and from 15 to 18 are approximately from 1.2 to 5.5 K, which are primarily attributable to the impact of heterogeneous surface properties. In some applications, such a level of error is acceptable, for example, the satellite precipitation retrievals from ATMS observations [8]. In contrast, the errors at temperatures sounding Channels 5 through 14, which are primarily used for hurricane warm core applications, are much smaller, predominantly within 1 K. Even so, certain limitation remains in the gap-filling technique for temperature sounding channels if the TC center (and associated warm anomaly) fell directly in between two ATMS swaths. In the above experiments of nine hurricanes cases, one extreme case is that the TC center (and associated warm anomaly) fell directly in between two ATMS swaths. As the artificially setting missed pixels are six, the errors (absolute values) at temperature sounding channels can increase to 2 K or higher depending sounding channel.

Overall, the DCT smoothing algorithm demonstrates significant deftness at filling in these synthetic gaps in the ATMS data record. Although the errors for window and lower sounding channels are relatively higher up to a few Kelvins, the maximum errors for temperature sounding channels related to hurricane vertical temperature profile retrievals is less than 1 K. Therefore, the gap-filled brightness temperatures at temperature sounding channels from 5 through 12 warrant the data quality and accuracy of the following gap-filled temperature vertical profile retrievals.

3. Development of ATMS-Based Atmospheric Temperature Retrieval Algorithms

Early in 2013, the ZW13 algorithm was developed for the retrieval of vertical atmospheric temperature field by using original ATMS SDR data at Channels 5 through 12 and has been successfully applied to Hurricane Sandy (2012) and other nine TCs. As a cross-track sounder, ATMS allows a broad swath of measurements to be taken, for example, 96 FOVs of ATMS SDR data per scan. An undesirable feature resulting from this scan method is that the measurements of brightness temperatures vary with scan angle because of changes in the optical path length through the Earth's atmosphere between the Earth and the satellite, which is referred to as the limb effect (Goldberg et al., 2001; Zhang et al., 2017). In the ZW13 algorithm, the vertical atmospheric temperatures, $(T(p))_{zw13}$, are derived by including a term inversely proportional to the cosine of the zenith

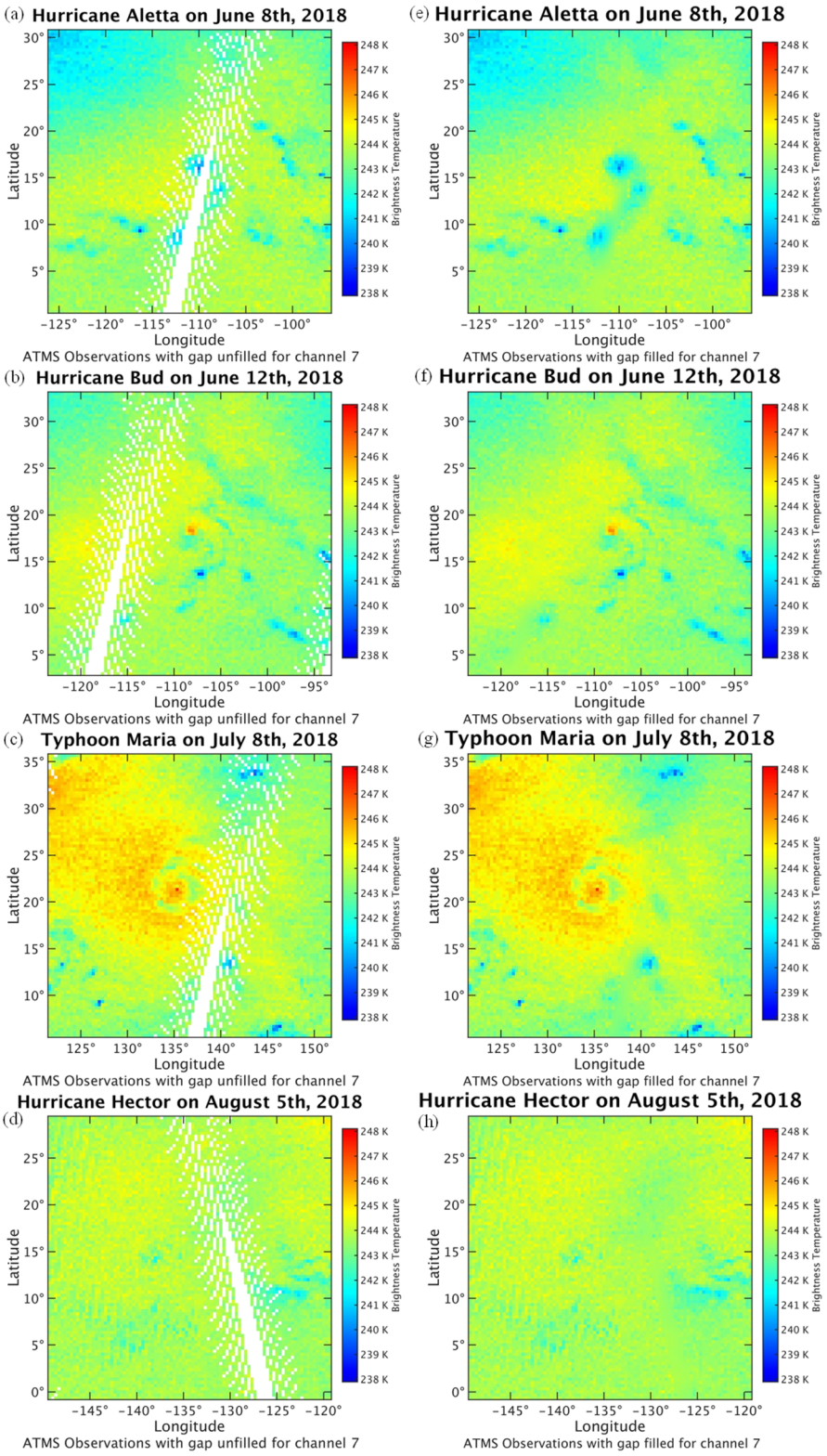

Figure 1. Comparison of ATMS brightness temperature distributions at Channel 7 with/without the gap filling by using the smoothing algorithm for observations of severe tropic storm events. (a) through (d) are four cases without the gap filling: (a) Hurricane Aletta on 8 June 2018. (b) Hurricane Bud on 12 June 2018. (c) Typhoon Maria on 6 July 2018. (d) Hurricane Hector on 6 August 2018. (e) through (h) are the same as (a) through (d), respectively, except they are the gap filling.

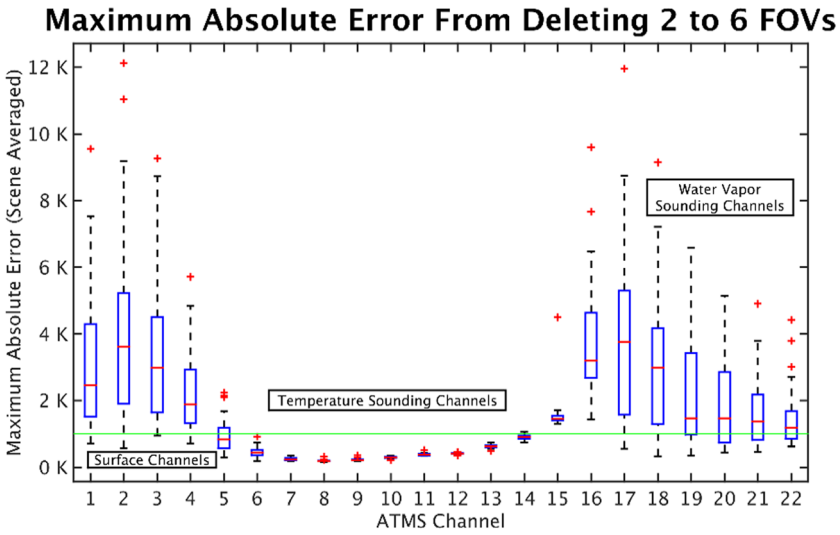

Figure 2. Box-plot of errors at each channel based on statistical analysis of 33 cases for the synthetic gaps, where the error is defined to be the difference between the predicted and measured brightness temperatures. On each box, the central mark indicates the median, and the bottom and top edges of the box indicate the 25th and 75th percentiles of the errors, respectively. The whiskers extend to the most extreme data points not considered outliers, and the outliers are plotted individually using the "+" symbol.

angle to account for the angle dependency of brightness temperatures, that is, the third term in the following equation.

$$(T(p))_{zw13} = A_0(p) + \sum_{i=N}^{12} A_i(p)T_b(v_i) + A_{SZ}(p)\frac{1}{cos(\theta)}, \tag{8}$$

where p denotes a given level among 21 pressure levels from 1,000 to 100 hPa for the retrieved temperature T; v_i is the frequency at channel i; T_b is original ATMS brightness temperature (i.e., without limb correction); the index "N" varies with clear skies ($N = 5$) or cloudy conditions ($N = 7$); A_0, A_i, *and* A_{SZ} are the derived regression coefficients using training data sets and are referred to the ZW13.

The ZW13 algorithm actually consists of two methods: the eight-channel algorithm for clear skies (hereinafter named as 8CHOC method) and the six-channel algorithm for cloudy conditions (hereinafter named as 6CHOC method). Both approaches use the temperature sounding channels as predictors, but 6CHOC uses six channels, and 8CHOC uses eight channels instead. However, considering the large residual errors for formulating the cosine term in vertical temperature retrievals, we handle it differently in this study. Our analysis has shown that the cosine term cannot entirely remove the angle dependency of retrieved atmospheric temperature field. Residual angle dependent error could be incorrectly identified as a warm core or temperature anomaly. In particular, the gap-filled ATMS SDR data employ the limb corrected data, where the observed brightness temperatures at all off-nadir FOVs are already adjusted to the nadir FOV (Zhang et al., 2017). On the other hand, the two algorithms in ZW13, that is, the 8CHOC and 6CHOC, are only applicable for open oceans while a hurricane is not making any landfall. However, as a hurricane approaches the coastline, it becomes challenging to detect clouds using the existing liquid water content (LWC) algorithm (Weng et al., 2003) because this algorithm is only applicable over oceans. Meanwhile, the heaviest rainfall of TC systems usually falls along or near the coastline (Goodyear, 1968). The Channel 7 used in the 6CHOC algorithm becomes sensitive to scattering and extinction of large rain drops, causing increased error and even some discontinuities in the derived hurricane warm core distribution from light to heavy rain. To reduce the artificial inconsistency owing to the 6CHOC algorithm deficiency in the warm core observation, the five-channel algorithm for coastal areas (hereinafter named as 5CHCA method) using five ATMS channels from 8 to 12 is further developed, and it is applied to all weather conditions.

Consequently, our study consists of the development of three new algorithms, that is, the 8CHOC (clear skies over open oceans), 6CHOC (cloudy conditions over open oceans), and 5CHCA (all weather conditions over

coastal areas) algorithm. The coefficients in the algorithms are derived by using the collocated European Centre for Medium-Range Weather Forecasts (ECMWF) analysis field (Dee et al., 2011; ECMWF IFS, 2018) and the limb-corrected ATMS observations during two hurricanes: Dorian and Lorenzo in 2019, two very typical and strong Atlantic hurricane cases with full hurricane life-spans and well-defined spatial coverages over open ocean and coastal areas. The ECMWF temperature analysis data are used as they are well validated against numbers of radiosonde measurements, with a bias within 1 K at levels from 100 through 1,000 hPa (Carminati et al., 2019; Ingleby, 2017). The limb-corrected ATMS data without gap filling are used to avoid the impact of any gap-filling errors. The training data sets used by the 8CHOC and 6CHOC are the ATMS data from 24 August 2019 through 31 August 2019 for Hurricane Dorian and the data from 23 September 2019 through 02 October 2019 for Hurricane Lorenzo. The data coverage per day is an area of ±15° in latitude/longitude around the storm center, where the ATMS data are entirely over oceans. The data for clear sky and cloudy conditions are used for the 8CHOC and 6CHOC training data, respectively. The 8CHOC algorithm is derived from over 100,000 data pairs under clear skies, and the 6CHOC algorithm is derived from over 14,000 data pairs under cloudy conditions. In contrast, the training data set for 5CHCA are the ATMS data over coastal areas during 01–06 September for Hurricane Dorian, with the spatial coverage of ±15° in latitude/longitude around the storm center. The 5CHCA algorithm is derived from over 60,000 data pairs over coastal areas. All regression coefficients can be made available to interested users upon request. The algorithms development and performance assessment are described as follows.

3.1. Development of Three Atmospheric Temperature Retrieval Methods

The retrieved temperature at a pressure level p under clear sky over open oceans is expressed as

$$T^{Clear}_{8CHOC}(p) = B_0(p) + \sum_{i=5}^{12} B_i(p) T_b^{LC}(v_i), \tag{9}$$

where T_b^{LC} is limb-corrected brightness temperature; the subscript "8CHOC" in T^{Clear}_{8CHOC} highlights that the algorithm uses eight ATMS channels and is applicable for open oceans, and the superscript "Clear" denotes that the algorithm works under clear skies; B_0 and B_i are derived regression coefficients at 21 levels from the surface to 50 hPa using the training data set.

Under cloudy conditions over oceans, as described in ZW13, surface and lower troposphere brightness temperatures can be contaminated by large rain droplets, especially precipitation in hurricane eyewalls. To minimize the influence of large brightness temperature bias attributable to heavy rainfall, brightness temperatures at Channels 5 and 6 are not used for the temperature retrieval under precipitation conditions. Therefore, the temperature at a pressure level p under cloudy conditions is as expressed below.

$$T^{Cloudy}_{6CHOC}(p) = C_0(p) + \sum_{i=7}^{12} C_i(p) T_b^{LC}(v_i), \tag{10}$$

where the subscript "6CHOC" in T^{Cloudy}_{6CHOC} highlights that the algorithm uses six ATMS channels and is applicable for open oceans, and the superscript "Cloudy" denotes that the algorithm works under cloudy conditions; C_0 and C_i are the derived regression coefficients at 15 pressure levels from surface to 250 hPa, although precipitating clouds hardly occur above the height of 6 km (approximately 450 hPa subject to actual atmospheric properties).

As a hurricane is over coastal areas before or after making a landfall, some of the ATMS data over the monitored hurricane domain might be over land. To reduce the inconsistency of the derived warm core distribution from light to heavy precipitations or discontinuity from ocean to land, a 5CHCA algorithm is developed, that is,

$$T^{All}_{5CHCA}(p) = D_0(p) + \sum_{i=8}^{12} D_i(p) T_b^{LC}(v_i), \tag{11}$$

where the subscript "5CHCA" in T^{All}_{5CHCA} highlights that the algorithm uses five ATMS channels and is applicable for coastal areas; the superscript "All" denotes that the algorithm works under all weather conditions; D_0 and D_i are derived regression coefficients at 21 pressure levels from surface to 50 hPa.

With the derived coefficients and formula from Equations 9 through 11, the temperature field can be retrieved from the gap-filled and limb-corrected ATMS data under all weather conditions over open oceans and coastal areas.

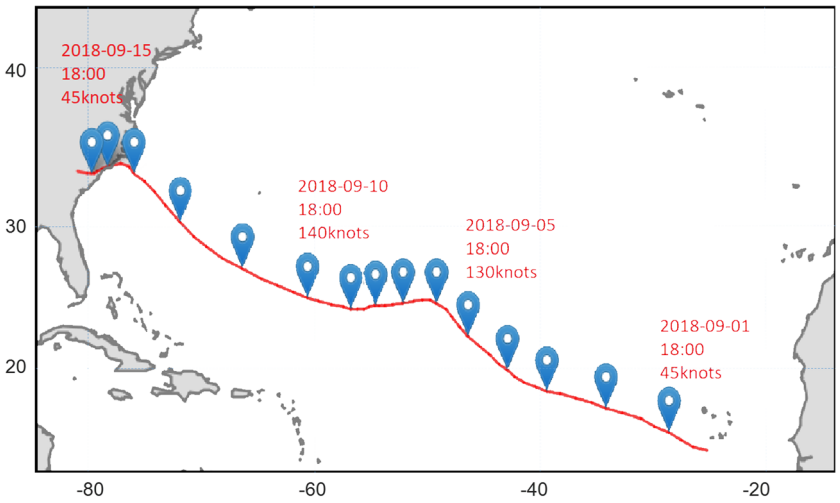

Figure 3. Hurricane Florence track spanning 1–15 September 2018.

3.2. Accuracy Assessment of Atmospheric Temperature Retrievals

Accuracies of the retrieved temperatures under all weather conditions over open oceans and coastal areas are assessed by applying the coefficients in Equations 9 through 11 to 15 days of ATMS data to retrieve vertical atmospheric temperatures of Hurricane Florence during 1–15 September 2018. Each day, a monitoring region used in this study is a box of 20° latitude × 20° longitude around the storm center. As shown in Figure 3, the monitored storm regions during 1–13 September were entirely over open oceans, and then over coastal areas from 14–15 September. In the following analysis, the 8CHOC and 6CHOC algorithms are applied to the ATMS data during 1 September to 13 September. The 5CHCA algorithm is applied to the ATMS data during from 14 September to 15 September. The retrieved atmospheric temperatures at different levels are compared with the collocated ECMWF analysis data at the same levels to compute daily-mean bias and standard deviation of biases per level.

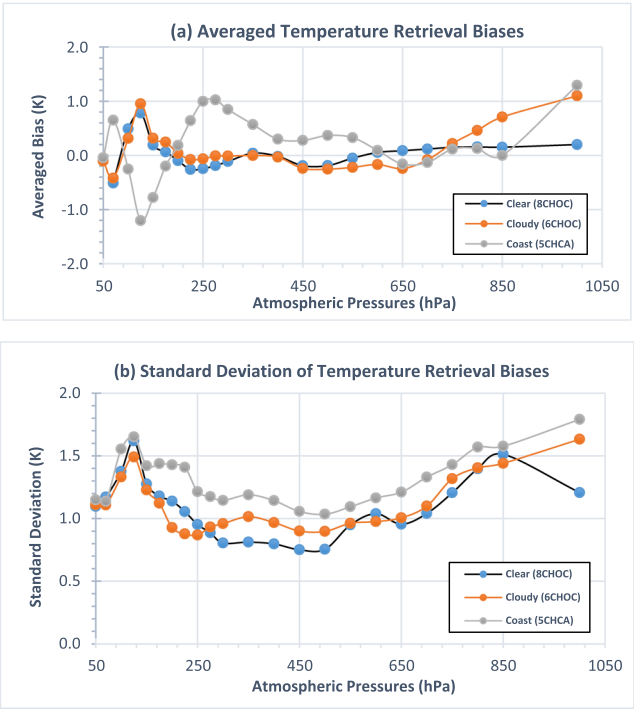

Figure 4. Averaged biases and standard deviations of the temperature retrievals against the ECMWF analysis data at different pressure levels by using the coefficients in Equation 9 for clear skies over open oceans, Equation 10 for cloudy conditions over open oceans, and Equation 11 for all weather conditions over coastal areas respectively. (a) The averaged biases. (b) Standard deviations. The results are computed using 13 days of the data over open oceans for Hurricane Florence (2018) spanning from 1 September through 13 September, and 2 days of the data from 14–15 September over coastal areas.

Figures 4a and 4b individually depict the averages of daily-mean biases and standard deviations of the biases over the related data period. Results demonstrate the good performance of the three algorithms in either bias or standard deviation against the ECMWF analysis. The biases in the three algorithms are within ±1 K at most levels, with the smallest bias found in the 8CHOC and the largest bias in the 5CHCA. Specifically, both the 6CHOC and 8CHOC algorithms show the biases within ±0.25 K for the levels between 200 and 700 hPa where hurricane warm core typically develops. Compared with the 8CHOC for clear skies, the 6CHOC and 5CHCA have an increased bias from the surface to 850 hPa primarily because of losing the information of two lower temperature-sounding channels (see Equations 10 and 11). Additionally, the 5CHCA displays increased biases at most levels compared with the other two methods, indicating the challenges of atmospheric temperature retrievals over land due to high surface emissivity. On the other hand, the three algorithms show degraded performance at the levels above 150 hPa, which is partially due to the lack of ATMS temperature sounding channels from 13 to 15 that can provide more temperature information around 100 hPa. Uncertainties in the ECMWF analysis at high levels could also be partially attributable.

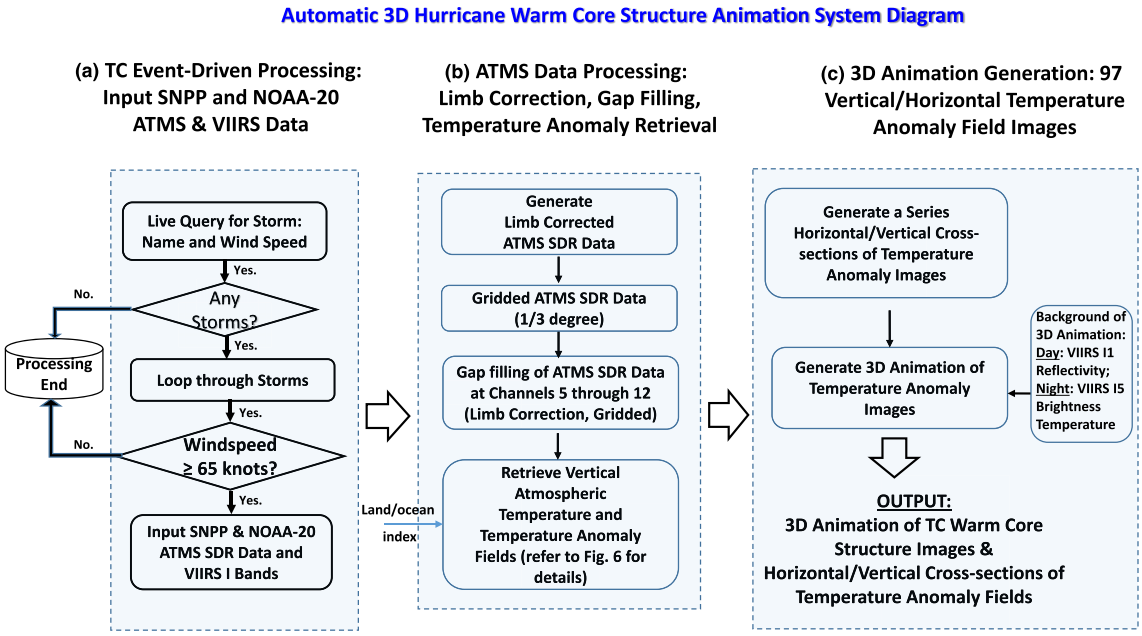

Figure 5. An automatic 3-D hurricane warm core system diagram.

For the standard deviations, similar conclusions are reached as the feature found in the bias. The standard deviations for the three algorithms are below 1.5 K at most levels, with the lowest in the 8CHOC and the highest in the 5CHCA. In particular, it is worthwhile noting that both the 6CHOC and 8CHOC algorithms exhibit the standard deviations that are below 1 K at the levels between 200 and 700 hPa. In contrast, the retrieved temperatures by the 6CHOC and 5CHCA show the standard deviation above 1.5 K below the 850 hPa pressure level (Figure 4b). This is not a concern because the algorithms are used typically at the lower and middle tropospheric levels.

Overall, over open oceans, the regression uncertainties in combination of the clear sky and cloudy algorithms are approximately less than 1.0 K at the midtropospheric levels, where warm core typically occurs, and increase up to 1.6 K at the other pressure levels. Over coastal areas, the uncertainties of the algorithm (5CHCA) are slightly larger than the other two algorithms (8CHOC and 6CHOC) by about 0.3 K. Last but not least, the three algorithms agree with each other with the averaged bias difference smaller than 0.5 K at most levels, ensuring the consistency of the warm core feature from clear to cloudy skies over oceans and from open oceans to coastal areas. The next section shows the development of the ATMS-retrieved 3-D HWCAS by using the derived coefficients via Equations 9–11, depending on weather and surface conditions.

4. Development of ATMS-Retrieved 3-D HWCAS

The 3-D HWCAS is developed by using the retrieved atmospheric temperature fields from the limb-corrected and gap-filled ATMS observations. Figure 5 illustrates the schematic flow chart of the HWCAS that comprises three key processing procedures. The first one is to ingest ATMS SDR data that is activated by a newly identified hurricane with wind speed higher than or equal to 64 knots. For Atlantic hurricanes, the information of approaching TC events is provided by the Atlantic 5-day of tropical weather outlook in NOAA Hurricane Center (NHC) (https://www.nhc.noaa.gov/gtwo.php/, accessed 25 March 2019; NOAA NHC forecast web tool, n.d.). This allows the system to run automatically due to the trigger of a hurricane event occurrence. The second one is the retrieval of atmospheric temperature anomaly vertical structure from the gap-filled ATMS SDR data. The last one is the generation of the 3-D animation consisting of 97 vertical/horizontal cross-section images of temperature anomaly. It takes about 1 hour (subject to computational resources) to complete the whole process from hurricane identification to 3-D animation production for an observed hurricane event. Since the first step of the processing is straightforward, the following subsections describe the last two processing steps in more details.

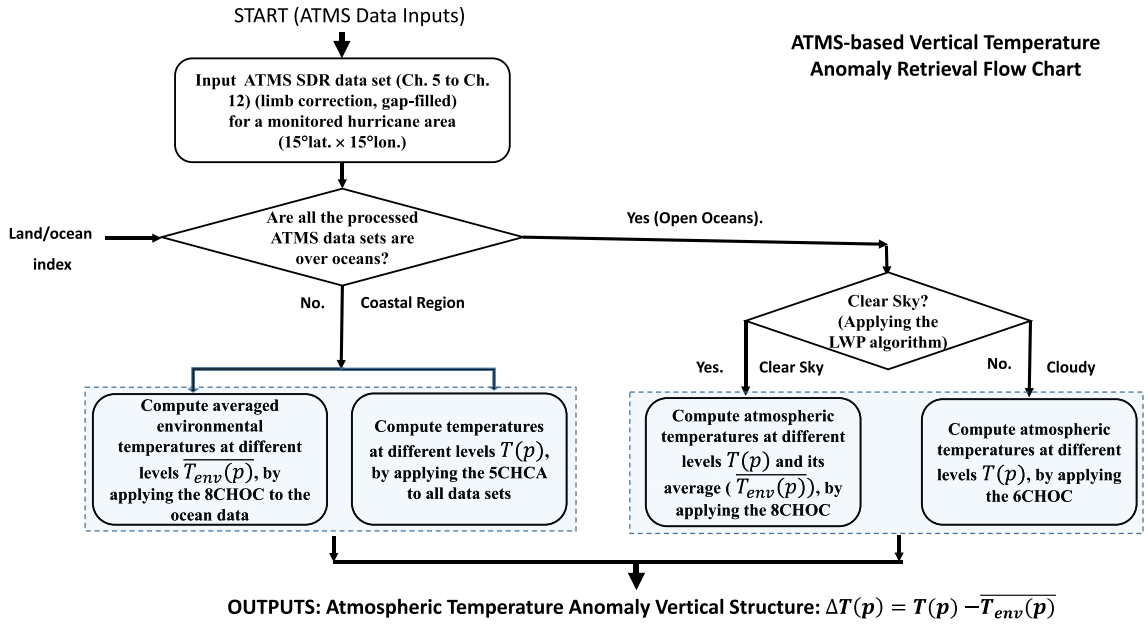

Figure 6. Schematic diagram of the data processing flow chart of the vertical atmospheric temperature anomaly field retrievals for a hurricane event over open oceans and coastal areas. In the chart, $\overline{T_{env}(p)}$, $T(p)$, and $\Delta T(p)$ represent averaged environmental temperature, atmospheric temperature, and temperature anomaly at a given pressure level, respectively.

The vertical structure of temperature anomalies is estimated by calculating the difference between the derived temperature field and the environmental temperature, as did in ZW13. The environmental temperature is defined as an average of derived temperatures using the 8CHOC algorithm in Equation 9 under clear skies over oceans within the monitored area. At the coastal area, the environmental temperature is defined as an average of derived temperatures within the regions beyond 5° from the storm center. The temperature field is derived using Equations 9–11, depending on weather and surface conditions. As described above, since all ATMS observations within the monitored hurricane area are over oceans, the 8CHOC in Equation 9 and the 6CHOC in Equation 10 are applied to the temperature retrievals under clear sky and cloudy conditions, respectively. When some ATMS observations within the monitored area are over lands, the 5CHCA in Equation 11 is applied to retrieve temperatures under all weather conditions. Figure 6 depicts the processing flow chart to calculate the vertical atmospheric temperature anomaly structures over open oceans and coastal areas according to different weather conditions.

To visually observe 3-D hurricane warm core structures, for an observed hurricane event, the HWCAS can produce the animation consisting of 97 2-D temperature anomaly images: 21 slices of the vertical cross-section images in latitude direction, 21 slices in longitude direction, 34 slices rotating around the center, and 21 slices of horizontal cross-sections from 1,000 through 100 hPa. The HWCAS has been successfully applied to a series of Atlantic hurricanes and Pacific typhoons in 2018. Among these, Hurricane Florence was a powerful and long-lived hurricane that was named on 1 September and dissipated on 19 September 2018, which caused severe damages in Carolinas. Using HWCAS, the warm core structure of Florence can be analyzed using NOAA-20 and SNPP ascending and descending ATMS data separately. In this study, the capability of the HWCAS in visualizing spatial and temporal structures of Florence warm core is demonstrated using the NOAA-20 ATMS ascending (daytime) observations below.

Figure 7 displays the horizontal cross-section of the ATMS temperature anomaly retrievals for Florence at several pressure levels on 10 September 2018. These images show that a well-defined warm core vertically extending approximately from 500 through 150 hPa was clearly observed. The maximum warm temperature anomaly in the warm core is 7.64 K occurring at 250 hPa level. Figure 8 presents four cross-sections of 2-D temperature anomaly images, revealing the vertical structure of Florence's warm core in a different view. Temperature fields below 550 hPa, which correspond to heavy precipitation regions in the eyewall, have colder temperatures than the upper temperature fields by a few Kelvin. This feature is related to attenuation of raindrops and large cloudy particles within heavy precipitations below the warm core levels.

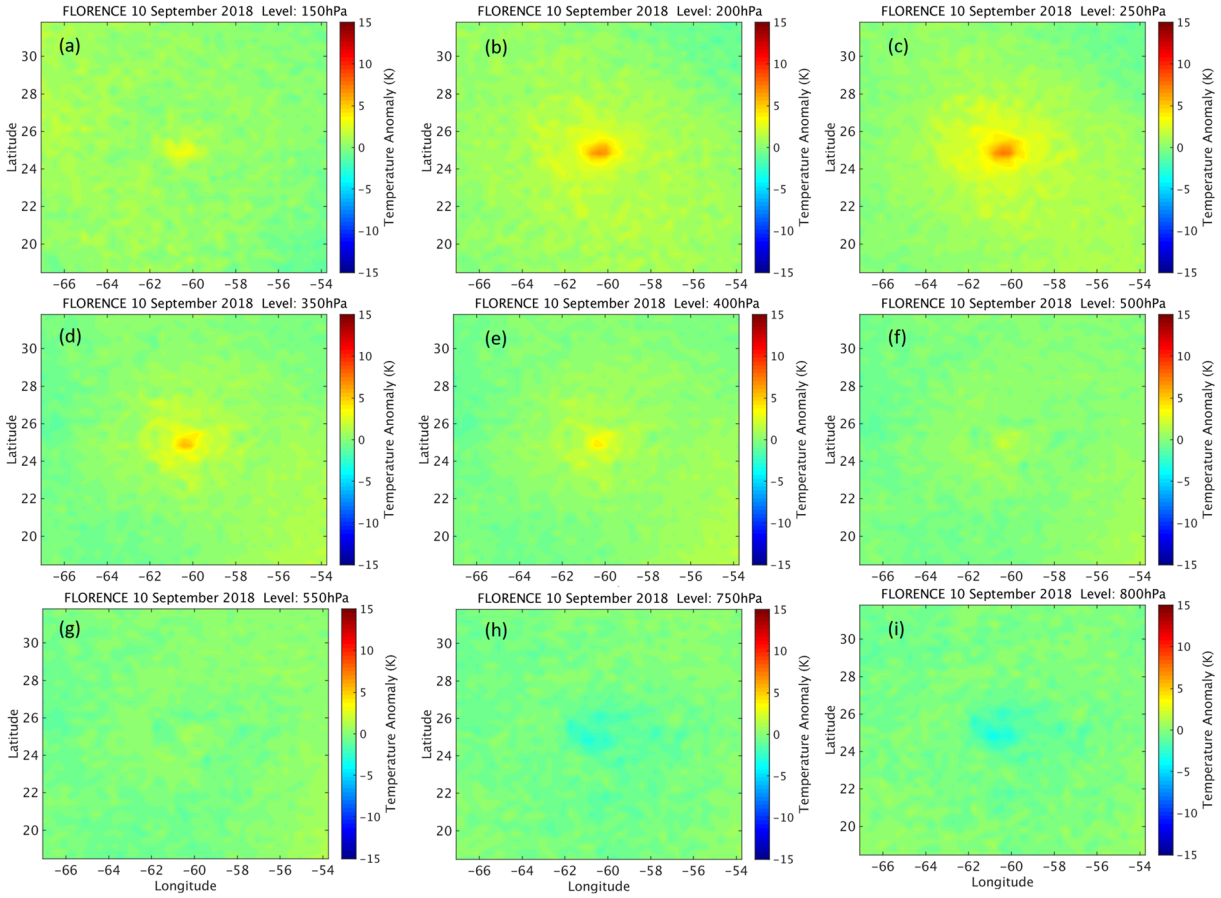

Figure 7. ATMS-retrieved temperature anomaly distributions from 15.2°N to 35.2°N in latitude and 50.6°W to 70.6°W in longitude at a few pressure levels for Hurricane Florence around 17:17 UTC on 10 September 2018. (a) 150 hPa; (b) 200 hPa; (c) 250 hPa; (d) 300 hPa; (e) 400 hPa; (f) 500 hPa; (g) 550 hPa; (h) 750 hPa; (i) 800 hPa.

Florence was a long-lived hurricane. To observe its day-to-day evolution, we apply the HWCAS to the ATMS ascending (daytime) observations during the hurricane development over oceans, (https://www.star.nesdis.noaa.gov/smcd/sew/FLORENCE.php). Figures 9a–9o provide retrieved temperature anomaly distributions for Hurricane Florence spanning 1–15 September 2018 correspondingly. In order to characterize the temporal changes of the warm core anomaly, Figure 10 shows the time series of "maximum" temperature anomaly at 300 hPa within the warm core area, at which level the peak warm core temperature anomalies usually occur. As implied from the time series, Florence experienced two stages of growths in terms of warm core intensity. The first intensification occurred during the period from 03 September through 05 September, with the maximum temperature anomaly of 4.36, 4.40, 4.48 K, respectively. It is also noted that an orbit gap occurred in the ATMS data on 05 September close to the storm center, which might result in an under-estimate of temperature retrievals or underestimate of the warm core size. After the intensification over 3 days, the hurricane weakened during 07 September through 09 September, and the maximum temperature anomaly on 08 September decreased to 2.47 K.

However, Florence reintensified since 08 September and grew into a Category 4 hurricane on 10 September as described above. The hurricane continued to intensify and reached a second peak on 13 September where warm core field extended vertically from 550 to 150 hPa (Figure 9m), and the temperature anomaly was approximately 11.98 K, much higher than the first intensification period of 03–05 September. This is because the storm is larger and the eye diameter is also larger so the sounder is seeing more of the warm core than the earlier period. After 13 September, the hurricane intensity became weakened, but its maximum temperature anomaly was still as large as 6.83 K on 15 September. This might imply that even during dissipation, clouds continued to maintain a strong warm anomaly around the 300 hPa level until the hurricane fully dissipated.

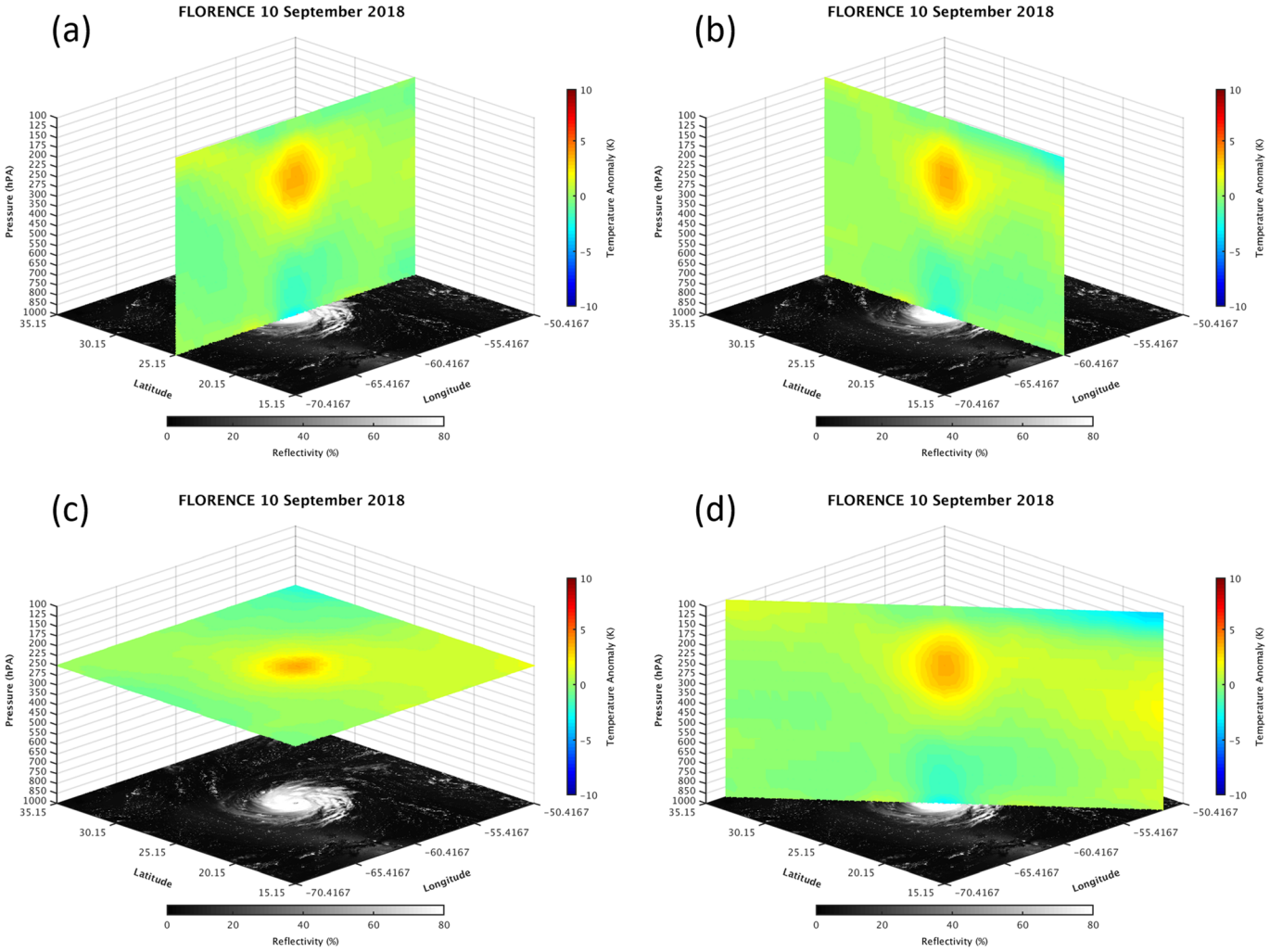

Figure 8. Four cross-sections of the 3-D hurricane warm core temperature anomaly animation for Hurricane Florence around 17:17 UTC on 10 September 2018.

Meanwhile, the warm core is no longer constrained by the TC eyewall thus expanding. This results in better viewing for the relatively coarse temperature sounding channels, while the loss of deeper convection in the core means less hydrometeor scattering. Additionally, the time series of the MSW provided by NHC best track data (https://www.nhc.noaa.gov/gis/best_track/) for Florence is added to Figure 10. It is interesting to notice that the whole maximum warm core experienced a weakening stage followed by a reintensifying stage similar to storm intensity or MSW, with a few temporal lead/lag between the maximum warm core and storm intensity. Besides the change of warm core intensity, its structure is pronounced from day to day as well, as shown in Figures 9a–9o. Overall, the HWCAS demonstrates certain capability to monitor he Florence's life cycle development from formation, intensification, weakening, reintensification, and dissipation.

To further validate the accuracy of the retrieved maximum temperature anomalies, we compared the retrieved maximum temperature anomaly to the ECMWF atmospheric temperature analysis field. Figure 10 includes the time series of maximum temperature anomaly that are computed using the ECMWF atmospheric temperature analysis field at 300 hPa where the retrieved maximum temperatures anomalies often occurred. The maximum temperature anomaly patterns from both ATMS retrievals and ECMWF analysis show a very similar hurricane lifecycle, including intensification, weakening, reintensification, and dissipation stages from 01 September through 15 September, although certain discrepancies in magnitude remains. The disparities could stem from several possible reasons, for example, ATMS-retrieval error, ECMWF model analysis error (Carminati et al., 2019; Ingleby, 2017), and the time

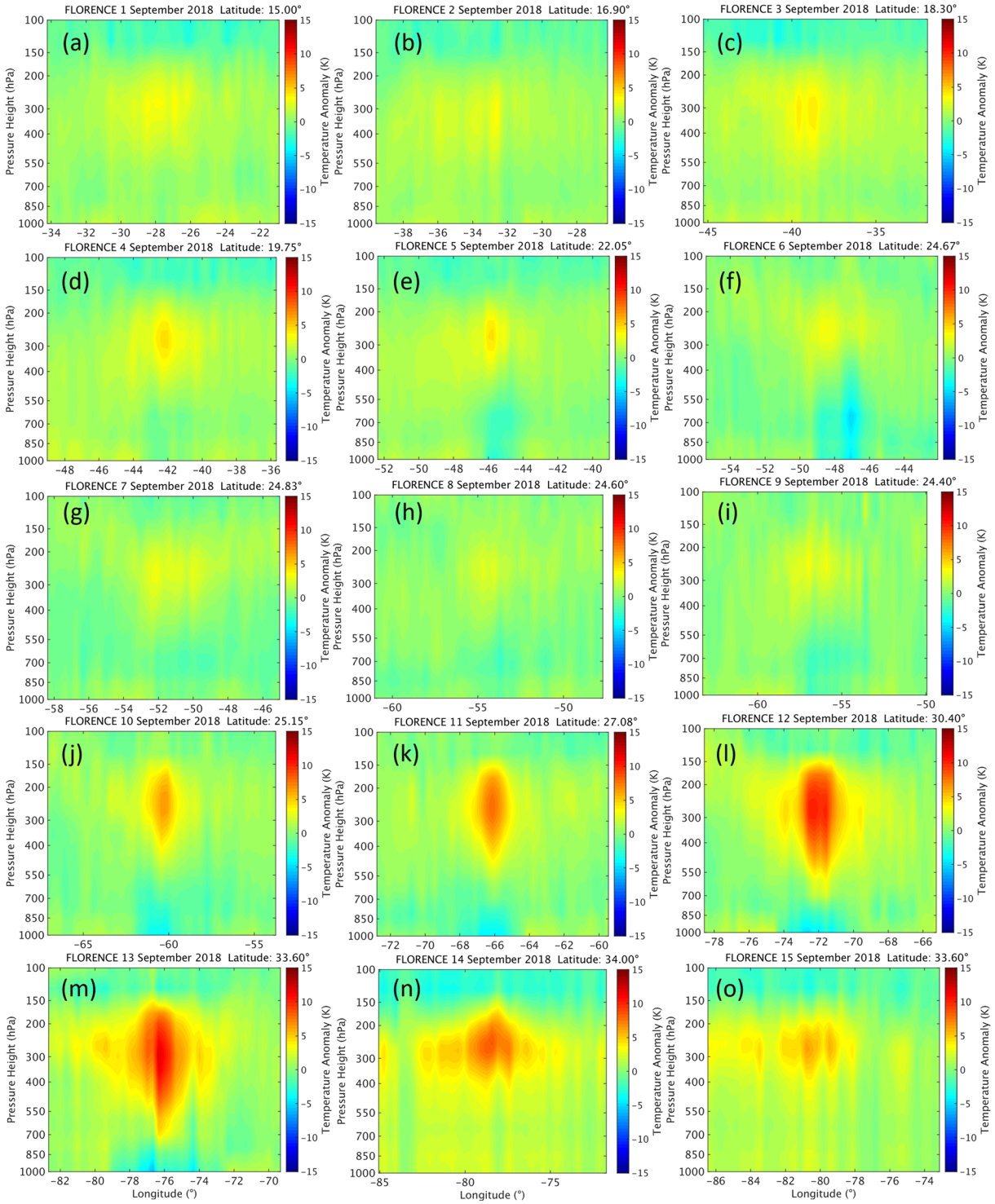

Figure 9. Evolution of ATMS-retrieved atmospheric temperature anomaly vertical structures for Hurricane Florence event from 1 September through 15 September 2018. (a) 01 September; (b) 02 September; (c) 03 September; (d) 04 September; (e) 05 September; (f) 06 September; (g) 07 September; (h) 08 September; (i) 09 September; (j) 10 September; (k) 11 September; (l) 12 September; (m) 13 September; (n) 14 September; (o) 15 September.

difference between ATMS observations and ECMWF analysis fields, and hydrometeor scattering and undersampling due to the resolution compared to the 20 km diameter eye. The composite error of retrieved temperature anomaly can be up to 2 K if the temperature anomaly for a given location is retrieved using gap-refilled data by the DCT smoothing algorithm. For example, as indicated from the

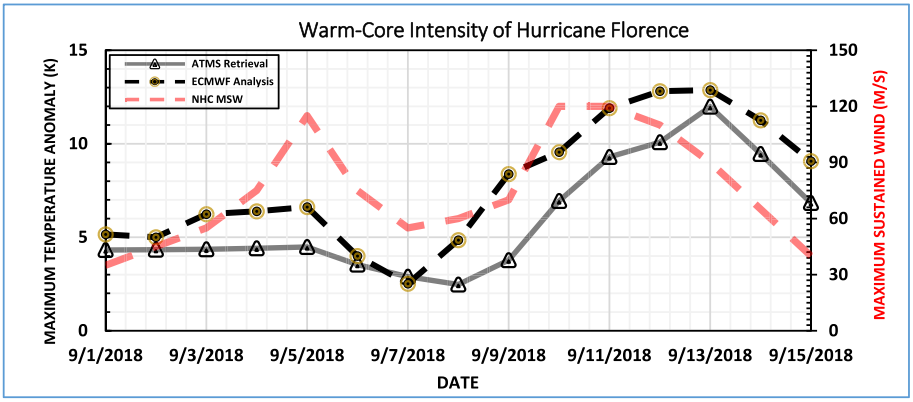

Figure 10. Time series of ATMS retrieved and ECMWF-analysis maximum temperature anomalies on the level of 300 hPa for Hurricane Florence spanning from 1 September through 15 September 2018. In the figure, the "ATMS retrieval" is computed using NOAA-20 ATMS ascending (daytime) observations with gap filling and limb correction. Additionally, the time series of the maximum sustained wind (MSW) provided by NHC best track data (https://www.nhc.noaa.gov/gis/best_track/) for Florence are shown in the figure.

above data analysis, ATMS temperature retrievals on 05 September could underestimate the warm core size because of the gap close to the storm center. On the other hand, the time difference between ATMS observations and ECMWF analyses are valid at the disparities. The daily ECMWF analyses include observations from 03:00, 09:00, 15:00, and 21:00 Coordinated Universal Time (UTC), while the equator crossing time of NOAA-20/ATMS observations is 13:00 local time. The ECMWF temperature analysis field that is the closest to the ATMS observation time is selected without interpolation for the comparison in Figure 10. Thus, the time difference between the model analysis and ATMS observation can be a couple of hours when hurricane could experience some structural changes.

The above results demonstrate that the HWCAS can successfully monitor the formation, intensification, weakening, reintensification, and dissipation stages of a hurricane warm core through temperature anomalies using the 3-D view animation. The time series of peak warm temperature anomaly agrees well with the temporal trend from the ECMWF analysis and shows a good correlation with the NHC MSW, albeit certain error in the gap-filled ATMS brightness temperatures especially when the gap occurs close to the hurricane center. Overall, our analysis has demonstrated the capability of HWCAS to visually monitor the spatial distribution and temporal evolution of hurricane temperature anomaly structures, based on the limb-corrected and gap-filled ATMS observations.

5. Summary and Conclusions

The ATMS brightness temperature SDR data for temperature sounding channels onboard SNPP, NOAA 20, and future JPSS-2 through JPSS-4 are valuable in visually monitoring spatial variability of hurricanes. However, orbital gaps at lower latitudes and missing observations at large zenith angles in the gridded data sets still cause uncertainty in their applications. To reduce such uncertainty, the existing DCT-PLS smoothing algorithm is used with its capability to fill the missing ATMS observations. Accuracy assessment of the gap-filled data set indicates that maximum errors of the filled values for temperature sounding channels are typically less than 1 K. Furthermore, the gap-filled brightness temperatures from Channel 5–12 were used to establish a new HWCAS to visually highlight hurricane temperature anomaly distribution in 3-D view. Temperature anomaly is retrieved using a combination of three new regression algorithms that are developed and improved based on the ZW13 study. The three algorithms are applicable to temperature retrievals of the following three scenarios, respectively: clear skies over open oceans, cloudy conditions over open oceans, and all weather conditions over coastal areas. The coefficients for the three algorithms are derived from collocated limb-corrected ATMS SDR data and ECMWF analysis field. The retrieving errors of temperatures at middle tropospheric levels where the warm core frequently occurs are typically within 1 K, although the error increases slightly at other levels. The highest error occurs at the surface pressure level and is approximately 1.5 K. The three algorithms also agree each other with the averaged differences less

than 0.5 K at most levels, illustrating consistent warm core feature from clear sky to cloudy over oceans, and from open oceans to coastal areas.

For an active hurricane event, the HWCAS can produce a NRT animation consisting of 97 temperature anomaly distribution images at different vertical/horizontal cross-sections to form a 3-D visualization for a given observation mode (ascending or descending) and satellite (SNPP or NOAA-20). As our test case of Hurricane Florence spanning 1–15 September 2018 reveals, the HWCAS demonstrates the capability to visually observe the formation, intensification, weakening, reintensification, and dissipation of a hurricane when it continuously monitors the hurricane's temperature anomaly fields from 01 September 2018 through 15 September 2018. In particular, it is worthwhile noting that the evolving time series of the ATMS-retrieved maximum temperature anomaly for Hurricane Florence agrees with the trend of the corresponding ECMWF analysis fields, indicating the ATMS retrievals were able to identify similar hurricane life stages of Florence during its lifespan, same as the ECMWF analysis. In addition, the retrieved warm core shows a strong correlation with NHC MSW in capturing the hurricane's weakening and intensifying process, although certain hours of temporal lead/lag remain between them. Therefore, limb-corrected ATMS observation appears to provide essential information for monitoring the evolution of TCs.

However, certain limitations may remain in the regression algorithms. The temperature retrieval uncertainty near the surface is relatively large especially under cloudy conditions or over coastal areas. The following factors may cause some uncertainty of the algorithm as a regression approach: (1) the dependence on training data, which may not capture some extreme events or events that fall outside the parameter space defined by the training set, and (2) the catastrophic failure of the algorithm in the event of a degradation or failure of one or more sounding channels. In such cases, the physically based algorithms such as the Microwave Integrated Retrieval System (MiRS) has more inherent flexibility and robustness and can usually quickly accommodate the loss of a sounding channel by simply turning it off in the minimization procedure. In addition, this study uses the ECMWF analysis data as validation data sets so that the performance of the algorithms might be partially tied to the skill of the ECMWF model to represent correctly the dynamic TC environment.

Nevertheless, as a fast supplementary or cross-validation tool to the physically based but sophisticated satellite retrieval systems such as MiRS [6], the HWCAS can offer an NRT 3-D view animation of hurricane warm core structure with a good accuracy by using a typical 45-minute processing time or much less time (subject to computational resources). Combination of ATMS descending observations on SNPP and NOAA-20 satellites could provide more consistent temporal and spatial coverage information of the hurricane. This information is not only critical for operational hurricane forecasts, impact evaluation, and decision making but also valuable for scientific investigations on hurricane origination, intensification, pathway migration, and beyond, before more accurately hurricane warm core information becomes available. In our future work, we will further improve the flexibility of the algorithm in the event of a degradation or failure of one or more sounding channels using artificial intelligence techniques. Moreover, we will investigate if the Backus-Gilbert enhancement can improve the accuracy of the ATMS observations near to the swath edges in comparison to the DCT-PLS smoothing algorithm. We also will use aircraft measurement data of atmospheric temperature fields from available field campaigns under hurricane events to improve the performance of the three algorithms.

Data Availability Statement

The original ATMS SDR and VIIRS SDR data sets that support the findings of this study are openly available in NOAA CLASS (NOAA CLASS web site, n.d.) at https://www.avl.class.noaa.gov/saa/products/search?datatype_family=VIIRS_SDR to search for the VIIRS Imagery Band 1 SDR (SVI01) that are used for hurricane visualization and https://www.avl.class.noaa.gov/saa/products/search?datatype_family=ATMS_TDR to search for the ATMS TDR data sets that are used for hurricane vertical profiling. Search specifications of include region of interest (±20° around any hurricane center), Start/End Dates and Time, Ascending/Descending modes for Day/Night observations. The ECMWF (reference number ECMWF) used in this study are obtained from the ECMWF data center at ftp://dissemination.ecmwf.int with requirement of a non-commercial use license. The global ECMWF atmospheric temperature analysis field data in GRIB format can be explored with specific date and time after logging in. The relevant hurricane geolocation, wind

speed, and surface pressure information used in this study are available from NOAA NWS National Hurricane Center at https://www.nhc.noaa.gov/gis/archive_forecast.php in shp and kmz formats, Reference Number NOAA NWS. Tropical cyclones are searchable by year and their NHC Storm Identifier, for example, Hurricane Florence is the storm al05 in 2018. The anomaly fields of Hurricane Florence that are derived from the ATMS TDR and used as demonstration example of our methodology are shared at the following anonymous ftp site ftp://ftp.star.nesdis.noaa.gov/pub/smcd/icvs/HWCAS in binary data format with data reader provided.

Disclaimer

The manuscript contents are solely the opinions of the author(s) and do not constitute a statement of policy, decision, or position on behalf of NOAA or the U. S. Government.

Acknowledgments

The authors thank the JPSS program for supporting JPSS-Integrated Calibration and Validation System (ICVS) project. The authors acknowledge Dr. Fuzhong Weng and Mr. Wanchun Chen for their preliminary tests of 3-D animation using the ATMS brightness temperature observations. Thanks also go to Dr. Xiaqiong Zhou for valuable scientific comments on the hurricane warm core structure features and their correlation with NHC maximum sustained wind. We appreciate Ms. Julie Price for her editorial review of the manuscript for grammar checking and correction. Last but not least, we thank a few anonymous reviewers for providing many valuable comments.

References

Ahmed, N., Natarajan, T., & Rao, K. R. (1974). Discrete cosine transform. *IEEE Transactions on Computers*, *C-23*(1), 90–93. https://doi.org/10.1109/T-C.1974.223784

Boukabara, S. A., Garrett, K., Chen, W. C., Iturbide-Sanchez, F., Grassotti, C., Kongoli, C., et al. (2011). MiRS: an all-weather 1DVAR satellite data assimilation and retrieval system. *IEEE Transactions on Geoscience and Remote Sensing*, *49*, 3249–3272. https://doi.org/10.1109/tgrs.2011.2158438

Boukabara, S. A., Garrett, K., Iturbide-Sanchez, F., Chen, W., Jiang, Z., Clough, S. A., et al. (2013). A physical approach for a simultaneous retrieval of sounding, surface, hydrometeor, and cryospheric parameters from SNPP/ATMS. *Journal of Geophysical Research: Atmospheres*, *118*, 12,600–12,619. https://doi.org/10.1002/2013JD020448

Carminati, F., Migliorini, S., Ingleby, B., Bell, W., Lawrence, H., Newman, S., et al. (2019). Using reference radiosondes to characterise NWP model uncertainty for improved satellite calibration and validation. *Atmospheric Measurement Techniques*, *12*, 83–106. https://doi.org/10.5194/amt-12-83-2019

Craven, P., & Wahba, G. (1978). Smoothing noisy data with spline functions. Estimating the correct degree of smoothing by the method of generalized cross-validation. *Numerische Mathematik*, *31*(4), 377–403. https://doi.org/10.1007/BF01404567

Dee, D. P., Uppala, S. M., Simmons, A. J., Berrisford, P., Poli, P., Kobayashi, S., et al. (2011). The ERA-Interim reanalysis: Configuration and performance of the data assimilation system. *Quarterly Journal of the Royal Meteorological Society*, *137*, 553–597. https://doi.org/10.1002/qj.828

Dolling, K., & Barnes, G. M. (2012). Warm-core formation in tropical storm Humberto (2001). *Monthly Weather Review*, *140*, 1177–1190. https://doi.org/10.1175/MWR-D-11-00183.1

European Centre for Medium-Range Weather Forecasts (ECMWF) (2018). IFS Documentation CY45r1, Reading, UK. Documentation available at https://www.ecmwf.int/en/publications/ifs-documentation

Ferraro, R., Meng, H., Zavodsky, B., Kusselson, S., Kann, D., Guyer, B., et al. (2018). Snowfall rates from satellite data help weather forecasters. *Eos*, *99*. https://doi.org/10.1029/2018EO096715

Garcia, D. (2010a). Robust smoothing of gridded data in one and higher dimensions with missing values. *Computational Statistics and Data Analysis*, *54*(4), 1167–1178. https://doi.org/10.1016/j.csda.2009.09.020

Garcia, D. (2010b). A fast all-in-one method for automated post-processing of PIV data. *Experiments in Fluids*, *50*(5), 1247–1259. https://doi.org/10.1007/s00348-010-0985-y

Goldberg, M. D., Crosby, D. S., & Zhou, L. (2001). The limb adjustment of AMSU-A observations. *Journal of Applied Meteorology*, *40*(1), 70–83. https://doi.org/10.1175/1520-0450(2001)040<0070:TLAOAA>2.0.CO;2

Golub, G., Heath, M., & Wahba, G. (1979). Generalized cross-validation as a method for choosing a good ridge parameter. *Technometrics*, *21*(2), 215–223. https://doi.org/10.1080/00401706.1979.10489751

Goodyear, H. V., & United States, Office of Hydrology. (1968). *Frequency and areal distributions of tropical storm rainfall in the United States coastal region on the Gulf of Mexico* (Vol. 7, pp. 1-48). US Department of Commerce, Environmental Science Services Administration, Weather Bureau: Washington, DC.

Ingleby, B. (2017). An assessment of different radiosonde types 2015/2016, ECMWF Technical Memoranda, https://www.ecmwf.int/en/publications

Kelly, G., & Thépaut, J. N. (2017). Evaluation of the impact of the space component of the Global Observing System through Observing System Experiments. *ECMWF Newsletter*, *113*, 16–28. http://www.ecmwf.int/publications/newsletters/pdf/113.pdf

Khayam, S. A. (2003). *The Discrete Cosine Transform (DCT): Theory and Application1* (pp. 5–8). Department of Electrical & Computer Engineering: Michigan State University.

Meng, H., Dong, J., Ferraro, R., Yan, B., Zhao, L., Kongoli, C., et al. (2017). A 1DVAR-based snowfall rate retrieval algorithm for passive microwave radiometers. *Journal of Geophysical Research: Atmospheres*, *122*, 6520–6540. https://doi.org/10.1002/2016JD026325

NOAA (n.d.). National Weather Service (NWS) National Hurricane Center (NHC) Tropical Cyclone Advisory Forecast, https://www.nhc.noaa.gov/gis/archive_forecast.php, accessed Oct 22, 2019.

NOAA CLASS (n.d.). National Oceanic and Atmospheric Administration Comprehensive Large Array-data Stewardship System (CLASS) (https://www.avl.class.noaa.gov/).

Strang, G. (1999). The discrete cosine transform. *Society for Industrial and Applied Mathematics Review*, *41*, 135–147. https://doi.org/10.1137/s0036144598336745

Tian, X., & Zou, X. (2016). ATMS- and AMSU-A-derived hurricane warm core structures using a modified retrieval algorithm. *Journal of Geophysical Research: Atmospheres*, *121*, 12,630–12,646. https://doi.org/10.1002/2016JD025042

Tong, X., Xu, J., Guan, Z., Han-Ching, C., Chiu, L. S., & Shao, M. (2017). An assessment of the impact of ATMS and CrIS data assimilation on precipitation prediction over the Tibetan Plateau. *Atmospheric Measurement Techniques*, *10*, 2517–2531. https://doi.org/10.5194/amt-10-2517-2017

Wahba, G. (1990). Spline models for observational data, Society for Industrial Mathematics; Philadelphia. Estimating the smoothing parameter, 45-65.

Wang, G., Garcia, D., Liu, Y., Jeu, R., & Dolman, A. (2012). A three-dimensional gap filling method for large geophysical datasets: Application to global satellite soil moisture observations. *Environmental Modelling & Software*, *30*, 139–142. https://doi.org/10.1016/j.envsoft.2011.10.015

Wang, Z., Montgomery, M. T., & Dunkerton, T. J. (2010). Genesis of pre-Hurricane Felix (2007). Part II: Warm core formation, precipitation evolution, and predictability. *Journal of the Atmospheric Sciences*, *67*(6), 1730–1744. https://doi.org/10.1175/2010JAS3435.1

Weng, F. (2018). *Passive Microwave Remote Sensing of the Earth: For Meteorological Applications (Wiley Series in Atmospheric Physics and Remote Sensing)*. Weinheim, Germany: Wiley-VCH. ISBN: 978-3-527-33627-2.

Weng, F., Zhao, L., Ferraro, R., & coauthors (2003). Advanced microwave sounding unit cloud and precipitation algorithms. *Radio Science*, *38*(4), 8086. https://doi.org/10.1029/2002RS002679

Weng, F., Zou, X., Sun, N., & coauthors (2013). Calibration of Suomi national polar-orbiting partnership advanced technology microwave sounder. *Journal of Geophysical Research: Atmospheres*, *118*, 11,187–11,200. https://doi.org/10.1002/jgrd.50840

Yang, H., & Zou, X. (2014). Optimal ATMS remapping algorithm for climate research. *IEEE Transactions on Geoscience and Remote Sensing*, *52*, 7290–7297. https://doi.org/10.1109/TGRS.2014.2310702

You, Y., Wang, N. Y., Ferraro, R., & Meyers, P. (2016). A prototype precipitation retrieval algorithm over land for ATMS. *Journal of Hydrometeorology*, *17*(5), 1601–1621. https://doi.org/10.1175/JHM-D-15-0163.1

Zhang, D.-L., & Chen, H. (2012). Importance of the upper-level warm core in the rapid intensification of a tropical cyclone. *Geophysical Research Letters*, *39*, L02806. https://doi.org/10.1029/2011GL050578

Zhang, K., Zhou, L., Goldberg, M., Liu, X., Wolf, W., Tan, C., & Liu, Q. (2017). A methodology to adjust ATMS observations for limb effect and its applications. *Journal of Geophysical Research: Atmospheres*, *122*, 11,347–11,356. https://doi.org/10.1002/2017JD026820

Zhu, T., & Weng, F. (2013). Hurricane Sandy warm-core structure observed from advanced technology microwave sounder. *Geophysical Research Letters*, *40*, 3325–3330. https://doi.org/10.1002/grl.50626

Zhu, T., Zhang, D.-L., & Weng, F. (2002). Impact of the advanced microwave sounding unit measurements on hurricane prediction. *Monthly Weather Review*, *130*(10), 2416–2432. https://doi.org/10.1175/1520-0493(2002)130<2416:IOTAMS>2.0.CO;2

Zhu, Y., Gayno, G., Delst, P. V., & Liu, E., Sun, R., Han, J., et al. (2017). Further development in the all-sky microwave radiance assimilation and expansion to ATMS in the GSI at NCEP, 21st International TOVS Study Conference, 29 November 5 December 2017, Darmstadt, Germany.

Zou, X., Weng, F., Zhang, B., Lin, L., Qin, Z., & Tallapragada, V. (2013). Impacts of assimilation of ATMS data in HWRF on track and intensity forecasts of 2012 four landfall hurricanes. *Journal of Geophysical Research: Atmospheres*, *118*, 11,558–11,576. https://doi.org/10.1002/2013JD020405